Modelling the partitioning of turbulent fluxes at urban sites with varying vegetation cover

Article

Published Version

Modeling the Partitioning of Turbulent Fluxes at Urban Sites with Varying Vegetation Cover

M. J. BEST

Met Office, Exeter, and Department of Geography, King's College London, London, United Kingdom

C. S. B. GRIMMOND

Department of Meteorology, University of Reading, Reading, United Kingdom

(Manuscript received 17 July 2015, in final form 20 May 2016)

ABSTRACT

Inclusion of vegetation is critical for urban land surface models (ULSM) to represent reasonably the turbulent sensible and latent heat flux densities in an urban environment. Here the Joint UK Land Environment Simulator (JULES), a ULSM, is used to simulate the Bowen ratio at a number of urban and rural sites with vegetation cover varying between 1% and 98%. The results show that JULES is able to represent the observed Bowen ratios, but only when the additional anthropogenic water supplied into the urban ecosystem is considered. The impact of the external water use (e.g., through irrigation or street cleaning) on the surface energy flux partitioning can be as substantial as that of the anthropogenic heat flux on the sensible and latent heat fluxes. The Bowen ratio varies from 1 to 2 when the plan area vegetation fraction is between 30% and 70%. However, when the vegetation fraction is less than 20%, the Bowen ratios increase substantially (2–10) and have greater sensitivity to assumptions about external water use. As there are few long-term observational sites with vegetation cover less than 30%, there is a clear need for more measurement studies in such environments.

1. Introduction

Over the last couple of decades, a number of models have been developed to represent urban land surface–atmosphere interactions, such as the Building Effect Parameterization (BEP; Martilli et al. 2002), slab urban energy balance model (Fortuniak 2003), multilayer urban canopy model (Kondo et al. 2005), Community Land Model–Urban (CLM-Urban; Oleson et al. 2008), and the Seoul National University urban canopy model (Ryu et al. 2011). Typically, these models are designed to represent the energy balance of the various facets that make up an idealized urban canopy. Often this idealized urban canopy is treated as a symmetric street canyon geometry with varying degrees of complexity, ranging from a bulk canyon (e.g., Best 2005), separate roof, walls, and road, with single (e.g., Masson 2000) or multiple (e.g., Krayenhoff and Voogt 2007) energy balances, and even intersections separate from street canyons (e.g., Kawai et al. 2009). While this may be a good representation of the central downtown areas of major cities, this design alone (i.e., without a representation of vegetation) does not capture the influence of vegetation present in many street canyons and abundant in the suburbs of many cities.

Vegetation also needs to be modeled for urban areas. Indeed, the first international urban model comparison experiment [Project for Intercomparison of Land-Surface Parameterization Schemes (PILPS-Urban)] concluded that for the two urban sites considered in the study (Vancouver and Melbourne), models that included a representation of vegetation performed much better in simulating the sensible Q_H and latent heat Q_E densities than models that neglected it (Grimmond et al. 2010, 2011; Best and Grimmond 2013, 2015). PILPS-Urban also concluded that the way in which the vegetation was modeled, that is, as a separate independent surface (e.g., Dupont and Mestayer 2006) or integrated within the urban street canyon (e.g., Lee and Park 2008), was not as important. However,

Corresponding author address: Martin Best, Met Office, Fitzroy Road, Exeter, Devon EX1 3PB, United Kingdom.
E-mail: martin.best@metoffice.gov.uk

DOI: 10.1175/JHM-D-15-0126.1

the main focus of PILPS-Urban results was a suburban site (Melbourne, Australia), so it is not clear how robust these conclusions are for other sites with varying fractions of vegetation within the footprint of the observations.

Observational data have quantified directly Q_H and Q_E and hence how the Bowen ratio β (i.e., $\beta = Q_H/Q_E$) varies with the vegetation fraction across a range of values (Grimmond and Oke 2002; Loridan and Grimmond 2012a). Here we investigate if an urban model that includes a representation of vegetation can reproduce this observed behavior.

In this study we use the JULES model (Best et al. 2011). It has been shown to perform well in simulating Q_H and Q_E compared to other models within PILPS-Urban (Best and Grimmond 2016). Here the model is used to simulate β for urban areas that range in plan area vegetation cover (i.e., two-dimensional vegetation cover as viewed from above) from 1% to 98% that correspond to 22 observational dataset footprint descriptions.

2. Methods

a. Observational sites

For this modeling study, evaluation data come from 22 observational tower sites (Table 1) where Q_H and Q_E were measured by eddy covariance in the inertial sublayer above usually uniform urban canopies. The measurements represent the neighborhood- or local-scale surface energy balance. The methods and analysis techniques used at each site are described in the papers corresponding to the individual sites (Table 1). The datasets include both short (<2 months) and long (>12 months) durations, with the longest (Baltimore) spanning 6 years. Most of the shorter datasets were collected in the summer months. For midlatitudes and semiarid climates, the summer months are the periods during which the vegetation is most likely to experience soil moisture stress and hence limited transpiration. The datasets with observations collected during the winter (Ouagadougou and Mexico City) are subtropical climates where the precipitation is typically less during the winter months. Hence, these are also the periods that are more likely to have soil moisture stress on the vegetation. Two rural sites outside of Basel (R1 and R2) were added to complete the spectrum of vegetation cover fractions modeled.

The surface characteristics affecting the measurements have a range from almost full vegetation cover to only 1% (Table 2). The surface cover data used in this study are from the literature. For the few sites with only the total vegetation amount reported, additional analyses were undertaken of available satellite imagery to subdivide this further.

For most of the sites the plan area proportions of vegetation and impervious surfaces (streets and buildings) combine to account for around 95% of the total area, with the exceptions of Tucson and Ouagadougou. These two sites have substantial areas of bare soil or unmanaged land (17% and 30%, respectively, which is modeled as bare soil). However, both these sites are in relatively dry climates, and so bare soil evaporation is unlikely to have a substantial contribution to Q_E, and hence β.

Forcing data for urban land surface models typically includes the downward components of both shortwave and longwave radiation; precipitation; surface pressure; and near-surface atmospheric wind, temperature, and humidity. Details on the observation of each of these variables at each of the measurement sites can be found in the references provided in Table 1. For many of the earlier datasets, the radiation components were not observed at the sites, but have been taken from nearby stations that make routine measurements or have been derived from empirical formulae.

b. Gap-filling for forcing data

As forcing data need to be continuous to undertake the simulations, any observational gaps need to be filled. For this study, the processed gap-filled forcing data from Loridan and Grimmond (2012b) are used where available. At sites where these processed data were not available, further gap-filling of the original observational datasets is required. While short periods (a few data values) can be filled using simple interpolation methods, this is not possible for longer periods. Hence, an alternative method is required.

For this current study, data from the Water and Global Change (WATCH) Forcing Data applied to ERA-Interim (WFDEI; Weedon et al. 2011, 2014) dataset have been used to fill any missing data gaps in the observational dataset. WFDEI spans the period from 1979 to 2012 and includes the data required to force land surface models. The dataset is global at 0.5° spatial resolution and has been derived using ERA-Interim (Dee et al. 2011) to downscale monthly observations from the Climatic Research Unit (CRU; New et al. 1999, 2000; Harris et al. 2014) to a temporal resolution of 3 h [see Weedon et al. (2011, 2014) for more details]. For precipitation, WFDEI has an alternative that is derived from the Global Precipitation Climatology Centre (GPCC; Schneider et al. 2014) for the monthly observations rather than CRU. In this study, the WFDEI dataset based on GPCC precipitation is used.

Given the global gridded nature of the WFDEI data (Weedon et al. 2011, 2014), it is quite likely that there

TABLE 1. Sources of observational data used in the analyses, with the main references for the data and the site characteristics. Local climate zones (LCZs) are according to Stewart and Oke (2012), as published in Grimmond and Christen (2012).

City and state or country	Site name	LCZ	Location	Period (length)	Data averaging period (min)	Instrument height (m)	References
Arcadia, California	Arcadia (93)	8	34.1°N, 118.0°W	July–August 1993 (40 days)	60	30.5	Grimmond and Oke (1995, 2002)
Arcadia, California	Arcadia (94)	6	34.1°N, 118.0°W	July 1994 (19 days)	60	32.8	Grimmond et al. (1996); Grimmond and Oke (2002)
Baltimore, Maryland	Baltimore	6	39.2°N, 76.7°W	May 2001 to December 2006 (2049 days)	60	41.2	Crawford et al. (2011); Loridan et al. (2011)
Basel, Switzerland							
Grenzach	Basel (R1)	D	47.5°N, 7.7°E	June–July 2002 (30 days)	10	1.5–28.0	Christen and Vogt (2004)
Village Neuf	Basel (R2)	D				2.0–3.3	
Allschwil	Basel (S1)	6				15.0–15.8	
Sperrstrasse	Basel (U1)	2				25.5–31.7	
Spalenring	Basel (U2)	2				33.0–37.6	
Chicago, Illinois	Chicago (92)	6	41.6°N, 87.5°W	July 1992 (13 days)	60	18.0	Grimmond and Oke (1995, 2002)
Chicago, Illinois	Chicago (95)	6	41.6°N, 87.5°W	June–August 1995 (57 days)	60	27.0	King and Grimmond (1997); Grimmond and Oke (2002)
Helsinki, Finland	Helsinki	Mixed	60.2°N, 24.9°E	September 2007 to December 2009 (853 days)	30	31.0	Vesala et al. (2008); Järvi et al. (2014)
Łódź, Poland	Łódź	2	51.8°N, 19.5°E	January 2001 to December 2002 (730 days)	60	37.0	Offerle et al. (2005a, 2006a,b); Pawlak et al. (2011)
Marseille, France	Marseille	2	43.2°N, 5.2°E	June–July 2001 (27 days)	60	39.0	Grimmond et al. (2004)
Melbourne, Australia	Melbourne	6	37.8°S, 144.9°E	August 2003 to November 2004 (475 days)	30	35.0	Coutts et al. (2007a,b)
Mexico City, Mexico	Mexico City	2	19.2°N, 99.1°E	December 1993 (7 days)	60	28.0	Oke et al. (1999); Grimmond and Oke (2002)
Miami, Florida	Miami	6	25.4°N, 80.2°W	May–June 1995 (26 days)	60	40.8	Newton (1999); Grimmond and Oke (2002); Newton et al. (2007)
Ouagadougou, Burkina Faso	Ouagadougou	—	12.2°N, 1.3°E	February 2003 (26 days)	60	10.0	Offerle et al. (2005b)
San Gabriel, California	San Gabriel	3	34.1°N, 118.0°W	July 1994 (22 days)	60	18.0	Grimmond et al. (1996); Grimmond and Oke (2002)
Sacramento, California	Sacramento	6	38.3°N, 121.3°W	August 1991 (10 days)	60	29.0	Grimmond et al. (1993); Grimmond and Oke (1995, 1999, 2002)
Tucson, Arizona	Tucson	7	32.1°N, 110.6°W	May–June 1990 (45 days)	60	25.6	Grimmond and Oke (1995, 2002)
Vancouver, Canada	Vancouver (VL92)	8	49.3°N, 123.1°W	August 1992 (15 days)	60	9.0	Grimmond and Oke (1999, 2002)
Vancouver, Canada	Vancouver (VS92)	6	49.3°N, 123.1°W	July–September 1992 (56 days)	60	14.1	Grimmond and Oke (1999, 2002)

TABLE 2. Sites ordered by increasing plan area cover of vegetation within the observational footprint. See Table 1 for site names and sources of data.

Site	Site code[a]	Trees (%)	Grass (%)	Total veg (%)	Buildings (%)	Streets (%)	Total built (%)	Bare soil (%)	Water (%)
Mexico City	Me93	1	0	1	54	44	97	2	0
Vancouver (VL92)	Vl92	3	2	5	51	44	95	0	0
Ouagadougou	Oa03	10	0	10	40	20	60	30	0
Marseille	Ma01	13	0	13	60	27	86	1	0
Basel (U1)	Ba02u1	11[c]	5[c]	16	54	30	84	0	0
Tucson	Tu90u	11	7	18	23	42	65	17	0
Łódź	Lo06[b]	22[c]	9[c]	31	30	40	69	0	0
Basel (U2)	Ba02u2	16[c]	15[c]	31	37	32	69	0	0
Miami	Mi95	7	27	34	35	29	64	0	2
San Gabriel	Sg94	12	25	37	29	31	60	0	4
Melbourne	Mb03m	23	15	38	45	18	62	1	0
Chicago (95)	Ch95	7	32	39	36	25	61	0	0
Vancouver (VS92)	Va08s[b]	9	35	44	31	24	55	2	0
Chicago (92)	Ch92	10	34	44	33	22	55	1	0
Sacramento	Sc91u	13	34	47	36	12	48	1	5
Helsinki	He05[b]	24	25	49	15	36	51	0	0
Arcadia (94)	Ar94	30	23	53	24	19	43	2	2
Basel (S1)	Ba02s1	21[c]	32[c]	53	28	19	47	0	0
Arcadia (93)	Ar93	32	24	56	22	18	40	2	2
Baltimore	Bm02	54	14	67	16	15	31	1	1
Basel (R1)	—	9[c]	82[c]	91	2	7	9	0	0
Basel (R2)	—	0[c]	98[c]	98	0	2	2	0	0

[a] Site code as published in Grimmond and Christen (2012).
[b] There are multiple observational datasets for the same site.
[c] The sites where judgment had to be used to determine tree and grass cover.

are inconsistencies between these data and those observed at the study sites. In particular, the long-term grid mean of WFDEI may not match a specific observational site mean. To assess this, periods with values in the observational dataset for the sites were used to determine if any biases existed in the WFDEI data. Any bias found was then applied to the WFDEI data to create values that could be used to gap fill the observational dataset while maintaining a consistent mean state.

While the forcing data are gap-filled, the observations used to evaluate the models are restricted to periods with valid observational data.

c. *Model description*

The model used for this study was the community land surface model Joint UK Land Environment Simulator (JULES; Best et al. 2011). This model uses a tiled approach to represent surface heterogeneity in land cover and by default includes five types of vegetation (two types of trees, two types of grasses, and shrubs) and four nonvegetation types (urban, lakes, bare soil, and permanent land ice), for which the urban tile represents the impervious surfaces of an urban environment.

This model has an aerodynamic resistance formulation based upon the Monin–Obukhov similarity theory (Monin and Obukhov 1954), while the resistance for surface water comes from either a simple water holding capacity for nonvegetation surfaces or stomatal resistance for vegetation based upon the photosynthesis model of Collatz et al. (1991, 1992). For vegetation, water is extracted from the soil based upon an exponential rooting depth profile, with the *e*-folding depth [the depth of soil that contains the fraction $(1 - e^{-1})$ of the roots] dependent on vegetation type. Trees have a rooting depth profile that primarily has roots in the bottommost layers, whereas grasses have roots that are primarily in the top soil layers. The leaf area index (LAI) for vegetated surfaces can vary temporally, but for this study they have been held fixed at their default values for all sites (Best et al. 2011).

Water infiltration into the soil is determined by the saturated hydraulic conductivity of the soil, with an additional enhancement factor that varies between vegetation types (Best et al. 2011). The soil is treated as a one-dimensional vertical column and is solved using a finite difference form of the Richards equation (Best et al. 2011). The thermal structure of the soil is modeled using the diffusion equation, and the energy equations include the vertical transport of the soil moisture along with phase changes of the water. The soil processes for both heat and water are modeled using the same four discrete layers and have increasing thickness with depth,

the layer depths being 0.10, 0.35, 1.00, and 2.00 m, respectively. The bottom boundary conditions for the soil are free drainage and a zero heat flux for energy conservation.

Results from the Protocol for the Analysis of Land Surface Models (PALS) Land Surface Model Benchmarking Evaluation Project (PLUMBER) community experiment showed the performance of this model for Q_H and Q_E, at a number of sites with natural surfaces, is comparable to many other land surface models (LSMs; Best et al. 2015).

Within this model there are three ways in which the impervious urban surface [i.e., ground (e.g., roads and parking lots) and buildings, excluding the vegetation and bare soil] can be represented, namely, the one-tile (Best 2005) and two-tile (Best et al. 2006) schemes and the Met Office Reading Urban Surface Exchange Scheme (MORUSES; Porson et al. 2010). The one-tile scheme represents an urban area as a bulk surface with parameters that represent a block of concrete. The two-tile scheme separates out the roofs of buildings from the street canyon, but the parameters for each surface are held constant and thus do not vary in space or time. The MORUSES scheme is similar to the two-tile scheme, except that the parameters and canyon turbulence are parameterized and depend upon the morphology of the urban area.

Results for all three versions were included in PILPS-Urban, although MORUSES was an early version that did not include vegetation. Results from the one- and two-tile versions of JULES were submitted by two modeling groups with different assumptions about their initial conditions of soil moisture. Results presented in Best and Grimmond (2014) showed that the initial conditions for soil moisture can have a substantial impact on Q_H and Q_E. However, Best and Grimmond (2016) show that four applications of JULES (a one-tile and a two-tile version run by two modeling groups) performed well in simulating Q_H and Q_E compared to other models in PILPS-Urban. For this study we have chosen to use solely the two-tile urban scheme within JULES, because Best et al. (2006) showed that this performed better than the one-tile version, but we have ensured that the initial conditions for the runs are appropriate by undertaking a spinup simulation, as described below.

d. Spinup strategy

Analysis of the results from PILPS-Urban showed that the initial conditions of soil moisture are important for the correct evolution of Q_H and Q_E (Best and Grimmond 2014). In addition, initial preparation work for the PLUMBER community benchmarking experiment (Best et al. 2015) identified that a 10-yr spinup period for soil moisture was sufficient provided the initial soil moisture was set to saturation, because gravitational drainage helps to remove excess water. However, if the soil moisture was set too dry before the spinup, then a 10-yr period was not sufficient for all climates.

A common method to spinup the soil moisture is to run the first year of the simulation repeatedly (e.g., 10 times). However, this results in soil moisture that is in equilibrium with the climatic conditions of the selected year and not necessarily a representative soil moisture that would have evolved from the climate prior to the study period. As many of the observational datasets considered in this study are shorter than a year, this method cannot be applied. Therefore, to be consistent between sites, an extended atmospheric forcing dataset (at least 10 years) prior to the period of the observational study for all sites was extracted from the WFDEI dataset used for gap-filling the forcing data (section 2b).

For each site the extracted WFDEI grid data were used to force JULES with a 30-min time step. The temporal interpolation from the 3-h resolution of WFDEI used a simplified Sheng and Zwiers (1998) algorithm within JULES. For radiation and precipitation data, a backward time averaging (i.e., time averaging that is valid at the end of the time period) that conserves the mean quantity is used, while for the other forcing variables a linear interpolation is used. The WFDEI temperature and humidity data are provided at screen level while the wind data are at 10-m height. However, the surface of the JULES model is not the true surface, but one that incorporates the displacement height (i.e., the displacement height is not explicitly represented), so the WFDEI data have been used to force the model without any changes to the height. This is acceptable because the spinup only needs to be in agreement with the previous mean climate, which can still be obtained from forcing at the heights of the WFDEI data.

Hence, for each observational site (Table 1) JULES was run for at least 10 years prior to the initial period of the observational study, forced with atmospheric data from WFDEI. The soil moisture state at the beginning of the spinup was specified as being saturated. The LSM was then run for the entire period to try to ensure that the soil moisture reached a correctly spun-up state. The soil moisture at the end of the spinup period provides the initial conditions of soil moisture at the start of the analysis period. The results from the analysis period are then taken from the continuous model simulation forced by the gap-filled data from the observations at the study sites, with the length of the model integration determined by the length of the observational dataset, which varied from 7 to 2049 days (Table 1).

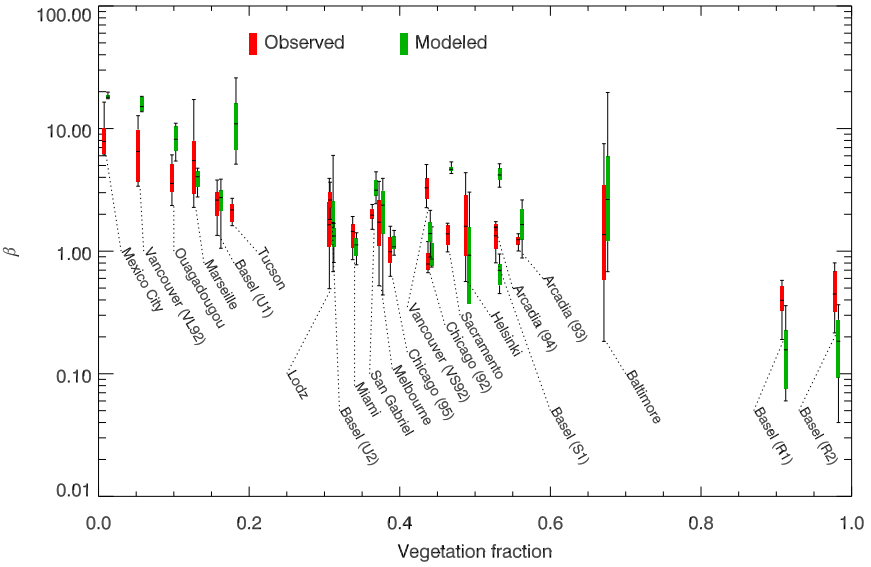

FIG. 1. Midday (1000–1400 LST) variability of observed and modeled Bowen ratio shown with the interquartile range (box), median (center lines), and 10th and 90th percentiles (whiskers).

e. *Model simulations*

Land-cover fractions were determined from publications about the sites (Table 2). For most the tree cover was separate from grass, but broadleaf or needleleaf were not specified. For the current study, it was assumed that trees were broadleaf and that the grass fraction was lawn.

Values of Q_H and Q_E from the model simulations were used to derive β around midday, based on the average of each flux density between hours ending at 1000 and 1400 local solar time (LST) on each day:

$$\overline{X} = \frac{1}{(N_{\text{days}} N_p)} \sum_{i=1}^{N_{\text{days}}} \sum_{j=1000}^{1400} X_{ij},$$

where X represents Q_H or Q_E, X_{ij} is the flux density at time j ($1000 \le j \le 1400$) on day i of the N_{days} of the simulation, N_p is the number of data points between 1000 and 1400 LST, and $\overline{X}$ is the midday average. The long-term Bowen ratio is the ratio of the averaged flux densities,

$$\beta = \frac{\overline{Q}_H}{\overline{Q}_E},$$

and was defined the same way for both the observations and model results, with missing observations periods omitted from both calculations. A midday value for β was used in preference to a daily average value because both fluxes are likely to be positive during the midday period, and Q_E (the denominator of β) is not usually close to zero, making the Bowen ratio more meaningful.

There could be many sources of errors in the model simulation that could impact all of the terms within the surface energy balance, such as incorrect surface albedos and unknown thermal heat storage properties of the building materials. Here the focus is the ability of the model to partition the surface fluxes between turbulent heat and moisture, hence β, and not the individual flux densities.

3. Results and discussion

Although the 18 short-duration datasets cannot be analyzed for seasonal variations, it is possible with the four multiyear datasets (Baltimore, Helsinki, Łódź, and Melbourne; see Table 1). However, as the results for each season are consistent with those for all available data (not shown), the analyses presented use all available data at each site.

The observed and modeled β values for each of the sites are shown in Fig. 1. The model results are in good agreement with observed β at a number of the sites [e.g., the two urban sites in Basel (U1 and U2), Miami, and Chicago (95); see Table 1 for sites], but at the majority of the sites β is overestimated by the model. At only one site is β substantially lower than the observed value [Vancouver (VS92)]. If β is too large, this implies that modeled Q_H is too large compared to Q_E, while a value that is too small implies that modeled Q_E is too large compared to Q_H.

In the following discussion we highlight cases where JULES and measurements disagree to explore further possible model improvements.

a. *Influence of garden irrigation*

One possible explanation for large β values in the JULES model is that the vegetation could be soil

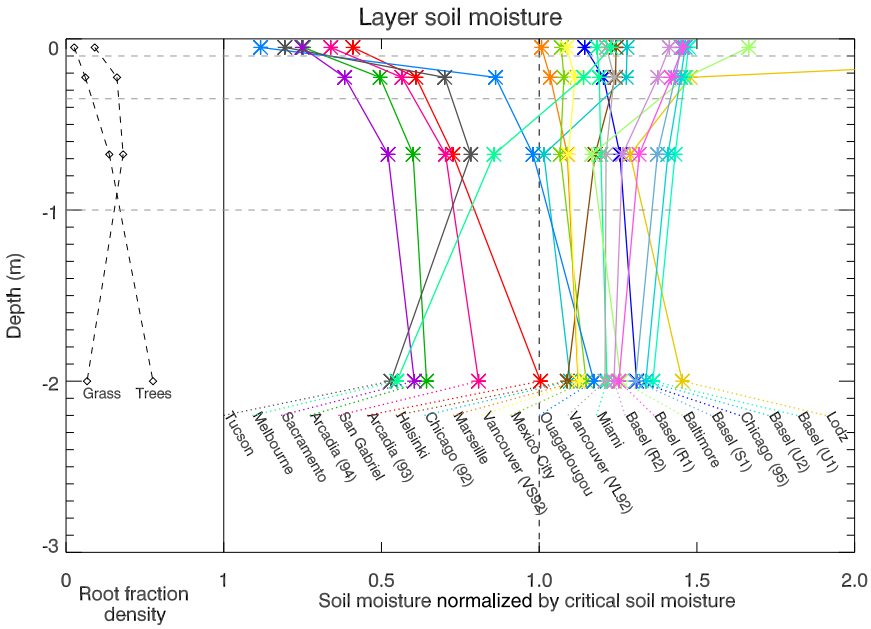

FIG. 2. Initial soil moisture profile used in the model simulations at each site (Table 1) derived from the spinup, and the model root density profiles for a grass and tree land-cover type. Horizontal dashed lines show the soil-level boundaries.

moisture stressed, and hence reduce the transpiration. To investigate the potential impact of the soil moisture, Fig. 2 shows the initial soil moisture profile (after the model spinup) within the soil column normalized by the critical point (the point at which vegetation starts to become soil moisture stressed within JULES; Best et al. 2011). A value less than one for any layer indicates that there is reduced soil moisture available to the roots in that layer, which will thus restrict the transpiration accordingly.

Different root density profiles are used within JULES that correspond to where soil moisture may be removed from by trees and grass (Fig. 2). For grass, soil moisture can be removed primarily from the second and third soil layers (0.10–1.00 m depth) within the model, while for trees the third and fourth soil layers (0.35–3.00 m depth) are the primary sources.

For many of the sites for which the model overpredicts β [Tucson, Melbourne, Sacramento, Arcadia (94), San Gabriel, Arcadia (93), and Ouagadougou; Fig. 1], the initial soil moisture profile (Fig. 2) was below the critical point for at least two of the four soil layers within the model.

The JULES model does not have a representation of irrigation. So to investigate the impact of the soil moisture stress on the vegetation, the model was rerun for each site, but with the unfrozen soil moisture (i.e., the liquid water phase that is available for transpiration) in every layer set to the critical point (or saturation minus frozen soil moisture if this was smaller) at each time step, that is, no soil moisture stress for the vegetation. This can be thought of as "optimal irrigation," equivalent to the minimum irrigation required to ensure that transpiration from the vegetation has no soil moisture limitation. The results of these simulations are shown in Fig. 3, along with the original default JULES simulations. Maintaining the soil moisture at the critical point in each layer reduces β to below that of the observations for most of the sites. Hence, the model can represent observed β values, but only if there is no soil moisture stress for the vegetation.

The spinup strategy (section 2d) used to initialize the soil moisture for each of the sites should have resulted in a reasonable initial state, based upon knowledge resulting from previous work (Best et al. 2015). However, for the work of Best et al. (2015) there were no anthropogenic influences at the study sites. At the urban sites of interest here, the additional soil moisture required to give a good simulation from the model could be the absence of an anthropogenic water injection. This may be watering by individuals to maintain their gardens (e.g., Sacramento) or street cleaning by the city to clear up after markets (e.g., Mexico City and Marseille). Such additions of anthropogenic water may also be regulated, for example, irrigation on alternating days (odd/even) in Sacramento (Grimmond and Oke 2002) or banning irrigation in Vancouver (VS92) because of drought. Under unrestricted irrigation conditions, Q_E

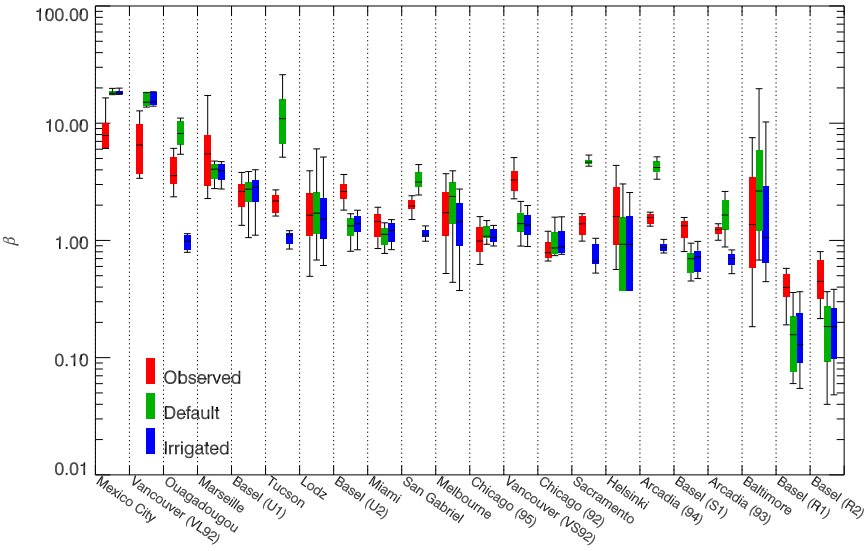

FIG. 3. As in Fig. 1, but for observed and JULES model runs—initial/default and with irrigation. Irrigation amount is based on model soil moisture fixed at the critical point. See text for further discussion. Sites are organized by increasing plan area fraction vegetated (see Table 2 for values).

closely follows irrigation (Grimmond and Oke 1986). Given the watering of gardens is to ensure healthy vegetation, it is not unreasonable to assume that the soil moisture for the majority of vegetated patches in an irrigated urban neighborhood is maintained around, or above, the critical point during dry periods.

b. *Influence of long-term soil water representation*

The simulations that maintained the soil moisture at the critical point also have a beneficial impact in reducing β at the Baltimore site, and to a much smaller extent for the Łódź site, even though the initial soil moisture after the spinup simulation was above the critical point for these sites (Fig. 2).

Both the Baltimore and Łódź sites are multiyear datasets, and as such, it is not only the initial soil moisture that will impact on overall β, but also the longer-term evolution of the soil moisture during the model simulation. Figure 4 (solid lines) shows the initial soil moisture profile (at the end of the spinup period), the final soil moisture profile at the end of the simulation, and soil moisture profiles at the end of each calendar year throughout the model simulation for each of the four sites with more than 12 months of data (Baltimore, Helsinki, Łódź, and Melbourne). By comparing the soil moisture profiles at the same time over consecutive years (i.e., the end of the calendar year), along with the initial and final soil moisture profiles from the model run, it is possible to identify if the modeled soil moisture has a drying or wetting tendency throughout the simulation. For instance, at the Baltimore site the bottom-model-level soil moisture (which has the long-term memory) is consistently drier each year throughout the simulation. The same is also true, but to a lesser extent, for the Łódź site. The Melbourne site has almost no change in bottom-layer soil moisture, but benefits from setting the soil moisture to the critical point because all of the soil moisture profiles are much lower than the critical point. For the Helsinki site there is no trend in the bottom-layer soil moisture, and hence the soil moisture state is not out of balance. The soil moisture for Helsinki is above the critical point for all of the profiles, which is consistent with there being no impact on β when setting the soil moisture profile to the critical point (Fig. 3).

The drying trends in soil moisture profile over the period of the simulations for both the Baltimore and Łódź sites could result from relatively dry conditions during the observational period compared to the previous years. However, it is more likely that the observational dataset has lower mean precipitation than the WFDEI dataset used for the spinup of the soil moisture (section 2d). Hence, the spun-up soil moisture is too wet relative to the mean climate of the observational data taken from the study site. So the soil moisture dries during the analysis period when the model is forced by the data from the observational site.

While it is not possible to compare the average precipitation between the observational dataset and that of WFDEI for the spinup period (because this is the period

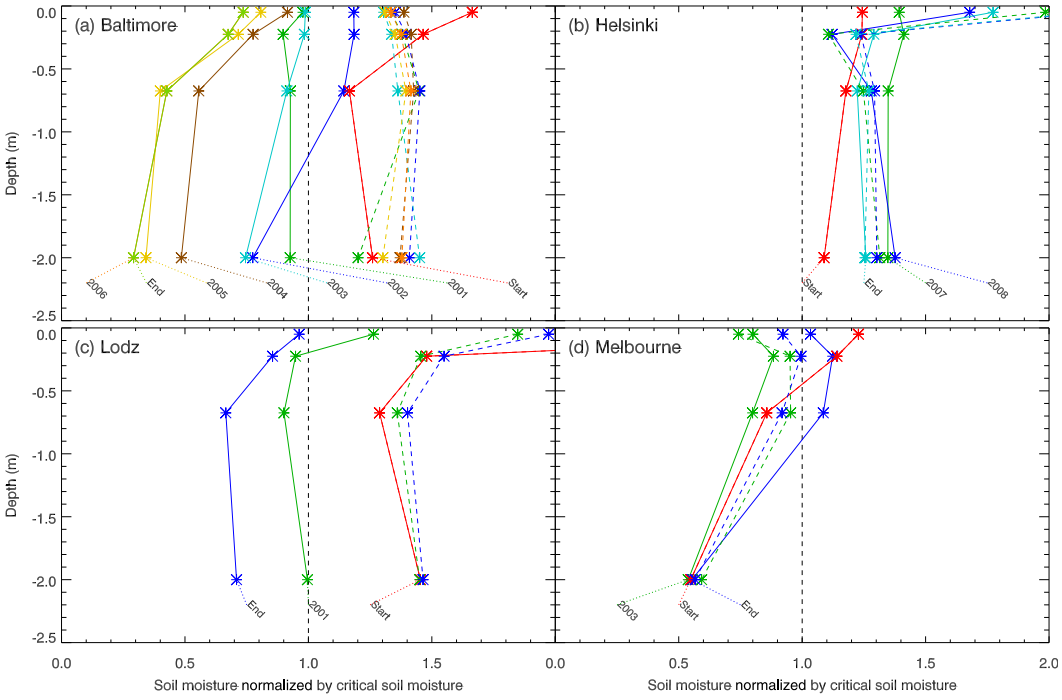

FIG. 4. Initial, final, and end of calendar year soil moisture profiles from model integrations at multiyear observational sites. The solid lines show the model profiles when forced with the local observational data. The dashed lines show the model profiles when forced with the WFDEI data. Note Baltimore, Helsinki, and Łódź are Northern Hemisphere sites, whereas Melbourne is Southern Hemisphere.

before the observational data starts), it is possible to compare precipitation during the observational period itself. Figure 5 shows the biases in precipitation for the WFDEI data relative to the observations from the four long-term sites. This figure shows clearly that there is more precipitation in the WFDEI dataset for Baltimore than in the observational dataset for the site. For the other three sites, there is less difference between the average precipitation from WFDEI and the observations from the sites, although for Łódź there is slightly more precipitation in WFDEI.

The bias for WFDEI compared to the observational data at the Baltimore site suggests that the precipitation in WFDEI is in error. However, the precipitation data in the observational dataset for Baltimore has not previously been analyzed, so the quality of these data is not known. To investigate if the issue is with WFDEI or the observational data at the study site, precipitation data were retrieved from synoptic stations close to the four sites: Baltimore–Washington International Airport (39.2°N, 76.7°W), Helsinki Airport (60.3°N, 25.0°E), Łódź Władysław Reymont Airport (51.7°N, 19.4°E), and Melbourne Airport (37.7°S, 144.8°E) (data obtained through the NOAA/National Climate Data Center: http://www.ncdc.noaa.gov/, using the HDSS Access System for Land-Based Station Data. Station codes are 72406, 02974, 12465, and 94866, respectively). The synoptic reporting stations follow the World Meteorological Organization (WMO) standards and as such include long-term measurements of precipitation.

The distribution of biases between the synoptic (Synop) and observational (Obs) data from the sites (Synop − Obs), and between WFDEI and synoptic data (WFDEI − Synop) are shown in Fig. 5. This shows clearly that for the Baltimore site, the WFDEI precipitation data are in closer agreement with the synoptic data than the observational data from the study site, although the synoptic station may have been included in the data analysis used to create the WFDEI dataset. This suggests that there may be errors in the previously unprocessed precipitation data for the Baltimore site. For the Łódź site, where the precipitation data from the observational site have previously been analyzed, the WFDEI dataset is also in better agreement with the synoptic station data, but the differences are much smaller than for the Baltimore site, that is, the three datasets are in better agreement.

The implications for Baltimore are that the original simulation using the observed precipitation forcing from the site (Fig. 1) had a negative bias in the observations (i.e., too little rainfall). To assess the impact of this, the model was rerun for Baltimore and Łódź with all atmospheric forcing data provided from the WFDEI

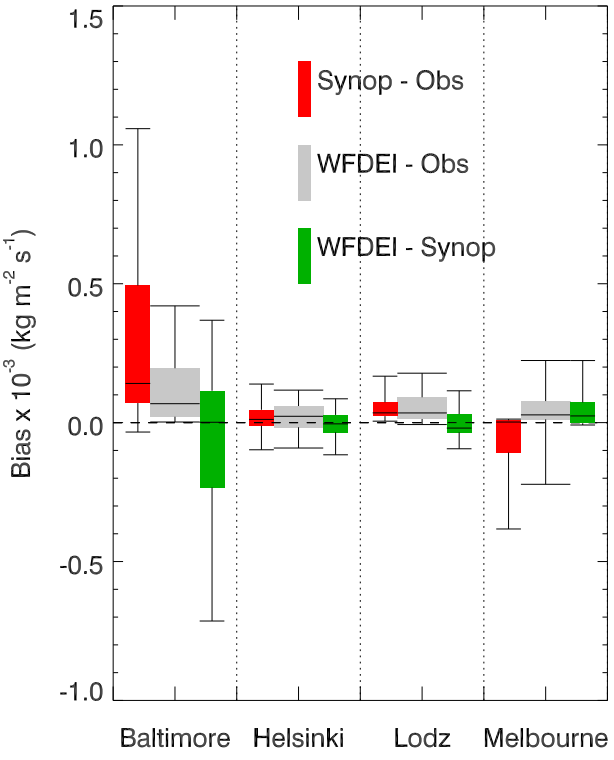

FIG. 5. Distribution (interquartile range, median, and 10th and 90th percentiles, as per Fig. 1) of bias in precipitation between WFDEI and observations at the study site, synoptic data and observations at the study site, and WFDEI and synoptic data for the multiyear sites.

dataset rather than the observational data from the study site (Fig. 6). All data were used, rather than just the precipitation data from WFDEI, to ensure consistency between the atmospheric data (e.g., to avoid simulating precipitation from WFDEI under clear sky conditions from the observational dataset at the study site). Any issues that arise from forcing the JULES model with data at the atmospheric heights of the WFDEI data have been neglected in this study. While such an assumption may not be valid, there are no other options available for obtaining consistent forcing data at more appropriate heights.

The greater precipitation from the WFDEI dataset maintains the soil moisture profile above the critical point for the Baltimore site, and the drying tendency between years is removed (dashed lines in Fig. 4). The removal of the restriction on evapotranspiration from the limitation of soil moisture means that the modeled β is reduced to values that are less than those observed (Fig. 6), which is consistent with many of the other sites in Fig. 3. The drying of the soil moisture profiles between years for the Łódź site is also removed with the WFDEI forcing (dashed lines in Fig. 4), but there is little difference in the resulting β (Fig. 6).

The remaining two sites in Fig. 4 (Helsinki and Melbourne) have smaller differences in soil moisture profiles between years from changing the data used for the forcing of JULES (cf. solid and dashed lines in Fig. 4). This is consistent with WFDEI data and the observations from the study site having similar precipitation averages (Fig. 5).

c. *Influence of bare soil surfaces*

While additional anthropogenically applied water might be responsible for maintaining vegetation transpiration rates at many of the sites, it is unlikely that unmanaged or bare soil areas are also irrigated. However, in the JULES model the different surface types share the same underlying soil. Hence, setting the soil moisture profile to the critical point during the simulation will also unrealistically increase the bare soil evaporation and provide an infinite reservoir of water, as conservation of mass is no longer constrained. As both the Ouagadougou and Tucson sites had a substantial fraction of bare soil or unmanaged land cover, they could be affected by this model limitation.

To investigate the impact on β, Q_H and Q_E were determined by the weighted average values from the individual surface types taken from two simulations. For vegetation surfaces, Q_H and Q_E were taken from JULES with the soil moisture set to the critical point, while for all other surfaces Q_H and Q_E were taken from the original default JULES. As there are no atmospheric feedbacks in these simulations, this is equivalent to irrigating only the vegetation part of the land cover.

The resulting β for the Tucson and Ouagadougou sites are shown in Fig. 6. The higher water availability for bare soil evaporation from the simulation with the soil moisture set to the critical point gave values of β that were substantially lower than those observed (Fig. 6). However, irrigating only the vegetated area reduced the unrealistically high β values from the original simulation for these sites (Fig. 6) but does not lead to such low values. Indeed, for Tucson the resulting β is in good agreement with the observed values, while for Ouagadougou the modeled β is higher than observed, but within the range of the observations.

d. *Influence of street cleaning*

The modeled β for the Mexico City and Vancouver (VL92) sites are substantially larger than the observed values (Fig. 1). Setting the soil moisture to the critical point has no impact on modeled β (Fig. 3) because the fraction of vegetation and bare soil within the footprint is small for both sites [1% and 2% for Mexico City and 5% and 0% for Vancouver (VL92)]. Hence, the available water for Q_E must come from a different source to the vegetation or bare soil surfaces.

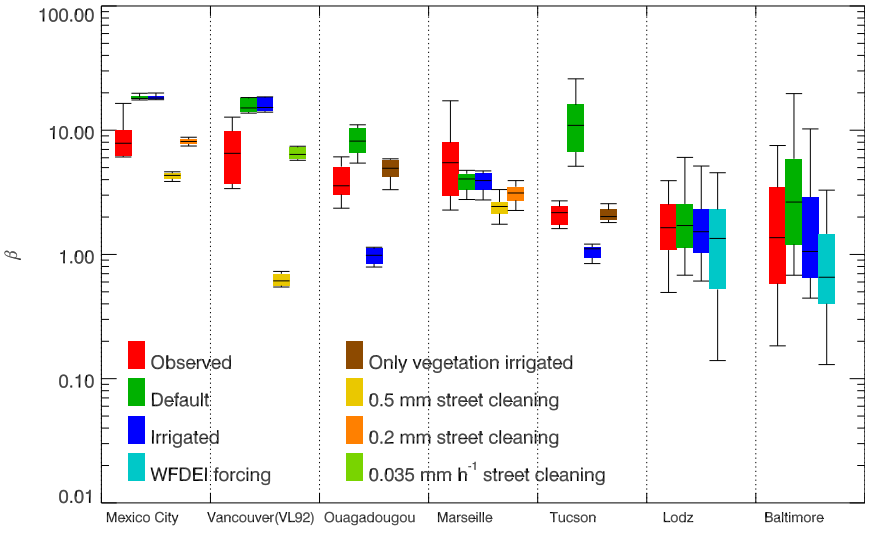

FIG. 6. As in Fig. 1, but for observed and JULES model runs—initial/default, with anthropogenic moisture added in various ways (irrigated, soil moisture fixed at the critical point; only vegetation irrigated, soil moisture held at critical point for vegetated land cover only; 0.5-mm street cleaning, artificial precipitation added to forcing in the morning amounting to a total of 0.5 mm; 0.2-mm street cleaning, artificial precipitation added to forcing in the morning amounting to a total of 0.2 mm; 0.035 mm h^{-1} street cleaning, artificial precipitation added to forcing each hour between 0900 and 1700 LT amounting to a total of 0.035 mm every hour), and using WFDEI forcing (WFDEI precipitation instead of observations at the study site). See text for further discussion. Sites are organized by increasing plan area fraction vegetated (see Table 2 for values).

At the Mexico City site, there was daily cleaning of the streets in the morning in preparation for the market (Oke et al. 1999). To understand if this source of water can explain a lower β in the observations at Mexico City, artificial precipitation was added to the forcing dataset between the hours of 0700 and 0800 local solar time (LST) each day. In addition, to ensure that the resulting water could only be retained on the street part of the urban surface and not the roofs, the water holding capacity of the roofs was set to zero. The amount of artificial precipitation each day was set to the maximum water holding capacity of the street, which is 0.5 mm in the default parameter settings of JULES (Best et al. 2011). Hence, this water reservoir within the street was set to its maximum value at this time, for each day of the simulation. In this scenario, the resulting modeled β is greatly reduced and results in values that are substantially below those observed (Fig. 6).

Information of the actual residual water that remained after the street cleaning process is not available from the field study, and so it is not clear if the correct amount of water was added to the street surface within the model. A sensitivity study, by varying the amount of artificial daily precipitation, shows that the optimal value of water held within the street to give the same average β as that observed was around 0.2 mm. (Fig. 6). Hence, it is feasible, and perhaps likely, that the source of water from street cleaning was responsible in reducing β to that observed.

Street cleaning was also undertaken at the Marseille site during midmorning after the market (Grimmond et al. 2004). The same artificial total precipitation required to fill the maximum water holding capacity of the street (0.5 mm) and the optimal value obtained for Mexico City (0.2 mm) were applied to the Marseille site, except that the artificial precipitation was added between 1000 and 1100 LST each day. In this case, the additional source of water has less of an impact because there is already a Q_E from the irrigated vegetation faction. However, β is reduced when the water from street cleaning is added (Fig. 6), with 0.2 mm of water resulting in a median that is in better agreement with the observations than 0.5 mm, as for the Mexico City site.

e. *Influence of advective fluxes*

No additional source of water at the surface was documented during the observational period for the Vancouver (VL92) site. Indeed, during this period Vancouver was experiencing drought conditions and was under an irrigation ban (Grimmond and Oke 2002). As such, the midday Q_E observed are small compared to the net all-wave radiation or the downward component of the shortwave radiation (Fig. 7). Small Q_E values

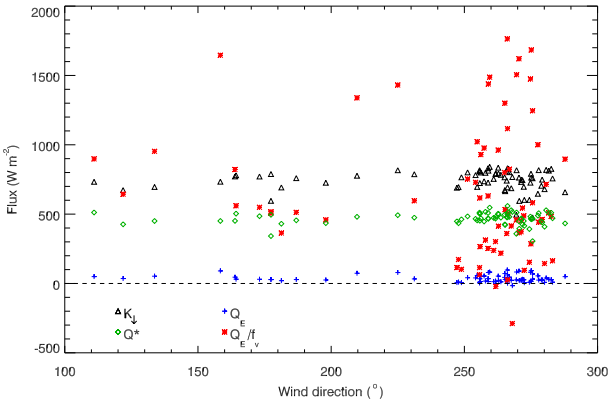

FIG. 7. Midday (1000–1400 LST) incoming solar radiation $K\downarrow$, net all-wave radiation Q^*, latent heat flux density, and latent heat flux density scaled by fraction of vegetation land cover within observational footprint (i.e., Q_E/f_v), against wind direction for the Vancouver (VL92) site.

typically have larger measurement error. This can be associated with measurements of low turbulence conditions by the sonic anemometer and/or low moisture availability measurements by the gas analyzer. Conditions of dew formation also increase measurement error. The lack of energy balance closure in observational datasets is frequently attributed to underestimation of the turbulent heat fluxes and a hysteresis effect in the storage heat flux (e.g., Leuning et al. 2012). In the current situation any corrections would proportionally increase Q_E and thus maintain or reduce β, so it is unlikely that the differences between the modeled and observed β values can be explained through observational errors.

As there was no precipitation during the observational period, the only water store at the land surface would be through the soil moisture. Since there was no bare soil surface within the source area of the observed fluxes, this implies that the only possible moisture source from the surface would be through transpiration from the vegetation. Figure 2 shows that the initial soil moisture profile for the Vancouver (VL92) site after the model spinup was such that there was no soil moisture stress on the vegetation, even though the site was actually in drought conditions. So the underestimation of Q_E, and hence high β, from the model cannot be explained by the initial conditions. This is also confirmed by the run with soil moisture held at the critical point, since this run does not impact on modeled β (Fig. 3).

If the observed midday values of Q_E at Vancouver (VL92) are scaled by the vegetation fraction f_v (i.e., assuming that the water vapor can only originate from transpiration from the vegetation fraction of the land cover), then the resulting Q_E from the vegetation is larger than the observed net all-wave radiation (Fig. 7), although for a rigorous comparison the net all-wave radiation should also be adjusted to reflect the value over just the vegetation. However, the rescaled evaporation (Q_E/f_v) is larger than the downward component of the shortwave radiation at times, which needs no such adjustment for vegetation fraction. Hence, it is very unlikely that Q_E observed at the Vancouver (VL92) site originated from soil moisture through transpiration within the turbulent source area of the eddy covariance observations on the tower.

As this was an industrial site, although there was no street cleaning documented, it is possible that there were some equivalent activities that could lead to a source of water on impervious surfaces. As such, a simulation with sufficient artificial total precipitation to fill the maximum water holding capacity of the street (0.5 mm) was applied for each hour between the working hours of 0900 and 1700 LT on each day. The addition of this water each hour provides a source reservoir that is large enough to reduce β to values far less than observed (Fig. 6). However, a sensitivity study shows that an amount of 0.035 mm each hour gives a modeled median of β that is close to that observed (Fig. 6). Hence, it requires only a small amount of water to be added each hour to explain the observed β, so it is possible that such a source of water is responsible for the observed evaporation.

An alternative explanation is that the moisture originates from the advective flux at atmospheric levels below the height of the eddy covariance system. Indeed, the wind direction around midday for most of the observational period was from the direction of False Creek, an inlet of the Pacific Ocean located from 600 m to 1 km upwind of the tower. A relatively warm and dry surface such as that within the observational footprint could give the buoyancy required to lift the advected vapor flux at low levels, hence leading to an observed midday average Q_E of 36 W m^{-2} at the site.

f. *Influence of a garden irrigation ban*

Vancouver (VS92) is the only site where the model substantially underestimates the observed β (Fig. 3). The observational period for this site coincided with Vancouver (VL92), so it was also experiencing drought conditions with an irrigation ban. However, the initial soil moisture profile for the model derived from the spinup has a soil moisture profile that is above the critical point, and hence the vegetation in the model is not soil moisture stressed (Fig. 2). This implies that there was too much precipitation in the forcing data from the WFDEI dataset during the spinup period, especially during the period immediately prior to the start of the observations at the study site.

Observations for the Vancouver (VS92) dataset were taken over 56 days, during which there was no precipitation in either the observational dataset or the WFDEI dataset. Therefore, it is not possible to make conclusions about any biases that there could be in the WFDEI dataset compared to the observations at the study site. In addition, the complex topography of the Vancouver area and its coastal location results in large precipitation gradients across the city (Oke and Hay 1998). As such, comparing the WFDEI dataset to a synoptic station would not necessarily result in any conclusions about precipitation biases compared to the observations at the study site. Moreover, the WFDEI dataset has a resolution of 0.5° and as such cannot be expected to give accurate precipitation values for specific parts in a region of such topographic heterogeneity.

The WFDEI dataset has two precipitation datasets based upon monthly climatologies from either GCPC or CRU (section 2c). In this study we have used the values from the GCPC data, but both climatologies are based upon a similar global precipitation gauge network. The number of gauges used for the climatology has a much lower density in the Vancouver (Canada) region compared to the coastal regions just to the south in the United States [see Schneider et al. (2014), their Fig. 5]. Also, New et al. (2000, their Fig. 1) show that the rain gauge density used for the CRU climatology decreased substantially between 1981 and 1995. Hence, it is quite likely that the heterogeneous nature of precipitation around Vancouver and the rain gauge density during the period of the observational campaign could have resulted in a lower-quality precipitation product for this site compared to other regions that have higher gauge densities. Thus, the 10-yr spinup for both Vancouver sites (VL92 and VS92) could be impacted.

Irrigation restrictions were also enforced during the summer at the Melbourne site. However, unlike the complete ban at Vancouver (VS92 and VL92), at Melbourne this involved no watering of lawns, while for trees and other vegetation automatic sprinkler systems were limited to the hours between 2300 and 0600 LST, and manual sprinkler systems limited to the hours between 0500 and 0800 LST and 2000 and 2300 LST. In addition, although the times during which irrigation could be applied were limited, the amount of water was not.

Calculating an average β for both the summer and winter at the Melbourne site shows that although β is slightly reduced in the winter, there is no impact on the ability of the model to simulate the observed values if it is assumed that the vegetation is sufficiently irrigated (not shown). The summer values for both observed and modeled β are similar to the overall results. Hence, the partial irrigation ban for the Melbourne site has little impact on the overall β compared to the complete ban at the Vancouver (VS92) site.

4. Conclusions

The initial soil moisture conditions have been shown previously to be critical for modeling sensible and latent heat fluxes in urban environments (Best and Grimmond 2015). In this study, initializing soil moisture with saturated conditions prior to a 10-yr spinup is shown to produce a soil moisture profile that is consistent with the model physics while enabling a realistic simulation, as long as there are no additional anthropogenic water sources such as irrigation. Hence, we recommend this for future studies when soil moisture profile observations are unavailable.

In addition, the WFDEI dataset is demonstrated, in general, to provide good-quality forcing data that can be used with this spinup strategy. While the quality of the precipitation data within the WFDEI dataset can vary depending upon the rain gauge density used to create monthly climatologies such as GPCC and CRU, it was of sufficient quality for most of the sites considered in this study. Hence, we also conclude that by using the WFDEI data and the 10-yr spinup strategy, it should be possible to initialize an LSM (including ULSM) at any site, as long as consideration is given to the density of rain gauges used for the monthly precipitation climatology, in addition to anthropogenic water sources.

In a summary of the results from PILPS-Urban, Best and Grimmond (2015) concluded that the important processes in the urban environment were the bulk reflection of the downward shortwave radiation, the influence of the urban morphology on the longwave radiation fluxes, and the vegetation processes for the distribution of the sensible and latent heat fluxes. This study has focused on the ability of JULES to simulate β across 22 observational datasets, that is, exploration of the model's ability to partition surface energy between the sensible and latent heat fluxes. Hence, the third physical process identified by Best and Grimmond (2015) is addressed. However, a good simulation of β does not necessarily imply that the model gives accurate values of Q_H and Q_E separately, which are also influenced by the radiative processes.

The results from the model show that at sites where the transpiration from vegetation is not restricted by limited soil moisture the model can reproduce observed β, while for the sites with limited soil moisture the model overestimates β compared to the observations. However, if we make the assumption that urban sites are irrigated to ensure that vegetation is not soil moisture stressed (i.e., urban residents maintain "healthy" gardens and parks), then the model is in good agreement with observed β at

these sites as well. The one exception, the Vancouver (VS92) site, was known to be in drought conditions with an irrigation ban in force. Hence, we conclude that when modeling vegetation within urban environments, it should be assumed that the vegetation is not soil moisture stressed, unless it is known to be a dry period with an irrigation ban in place. Given these assumptions, the JULES model is able to represent the observed urban β over the range of plan area vegetation fractions considered in this study (Fig. 8a).

The possibility of an irrigation ban within urban environments makes the modeling of urban vegetation complex, but important. The availability of soil moisture for transpiration is not a physical condition as it is for the rural environment, but becomes a combination of physical and social conditions. Factors such as population density (i.e., water demand), wealth (e.g., artificial water storage applications), national infrastructure (i.e., transport of water), and stakeholder requirements (e.g., city dweller water use vs agricultural irrigation) may all influence the political decision-making with regard to an irrigation ban. For instance, compare the different urban water use practices and water availability in the climates of Ouagadougou (Offerle et al. 2005b), Marseille (Grimmond et al. 2004), Vancouver and Chicago (Grimmond and Oke 1999), and Arcadia and San Gabriel (Grimmond et al. 1996). Hence, we conclude further studies are needed to investigate the implementation of irrigation bans and their impact on the surface energy and water balance for urban areas.

Irrigation of vegetation is not the only anthropogenic moisture source that can influence the turbulent fluxes of heat and moisture within the urban environment. This work has shown that activities such as street cleaning can provide a source of water that can moderately increase Q_E. Hence, all possible sources of anthropogenic water are important and need to be represented within an urban land surface model. Furthermore, the impact of such anthropogenic water injections suggests that they are at least as important as the anthropogenic heat flux density on the terms in the surface energy balance for urban areas.

For well-irrigated vegetation, there is little change in β for sites with vegetation cover between 30% and 70% (Fig. 8a). While there is some day-to-day variability at the sites, the average β is typically in the range of 1–2. The two rural sites near Basel with almost total vegetation cover (R1 and R2) have β values less than one, which is typical for rural locations. However, as the vegetation fraction decreases below 20%, β increases substantially, with a maximum value of around eight for the most densely built-up urban site studied here (Mexico City). However, for this site β was reduced because it was controlled by water availability from street cleaning. Also, for the secondmost impervious site [Vancouver (VL92)], the observations may have been influenced by water added to the surface in a similar manner to street cleaning, or atmospheric advection of moisture into the source area at levels below the height of the observations. As such, it is possible that without these additional sources of moisture, β could be as large as 20 for urban sites with little vegetation during summertime. However, Offerle et al. (2006b) suggested that sparse vegetation may well be exposed to higher vapor pressure deficits and higher temperatures, while isolated trees are exposed to higher photosynthetic active radiation (PAR), which could increase transpiration. Also, Meier and Scherer (2012) concluded that trees surrounded by a high fraction of impervious surfaces showed consistently higher canopy temperatures. In addition, we have made no attempt to distinguish between native and nonnative vegetation. High latitude, midlatitude, semiarid, and tropical vegetation all have different characteristics that could influence the results for sparse vegetation cover. Hence, additional observational studies are required for urban environments with sparse vegetation and no additional anthropogenic water injections, to determine the behavior of vegetation in such environments.

If we consider how Q_E varies with vegetation fraction, we find that as a proportion of the available energy at the surface, there is a step change around vegetation fractions of 20%–30% (Fig. 8b). This step change is also seen when scaling Q_E by the incoming all-wave radiation (Fig. 8c). This result agrees with Loridan and Grimmond (2012a), who found such a step change in the scaled Q_E against their active vegetation index. Furthermore, when scaled by the incoming all-wave radiation, there is also a step change in Q_E with almost total vegetation cover (70%–90%, Fig. 8c), or little built area cover, although this step change is not seen in Q_E as a proportion of the available energy at the surface. This suggests that there could be a step change in the net heat storage flux density for small built fractions, as confirmed by the results of Loridan and Grimmond (2012a), who showed a step change in the storage heat density for changes in active built index. Hence, we conclude that the sensitivity of Q_E, and hence the Q_H through the available energy at the surface, is greatly increased when there is little vegetation cover, while the sensitivity of the heat storage is greatly increased when there is little built area cover.

The results from this study suggest that an urban land surface model, such as JULES, can reproduce the observed β values of urban sites. However, the sensitivity of the urban energy balance at sites with low fractions of vegetation land cover, or low fractions of built area, suggests that further studies are required for urban environments with less than 30% vegetation cover and less than 30% built area cover. This can only be achieved if

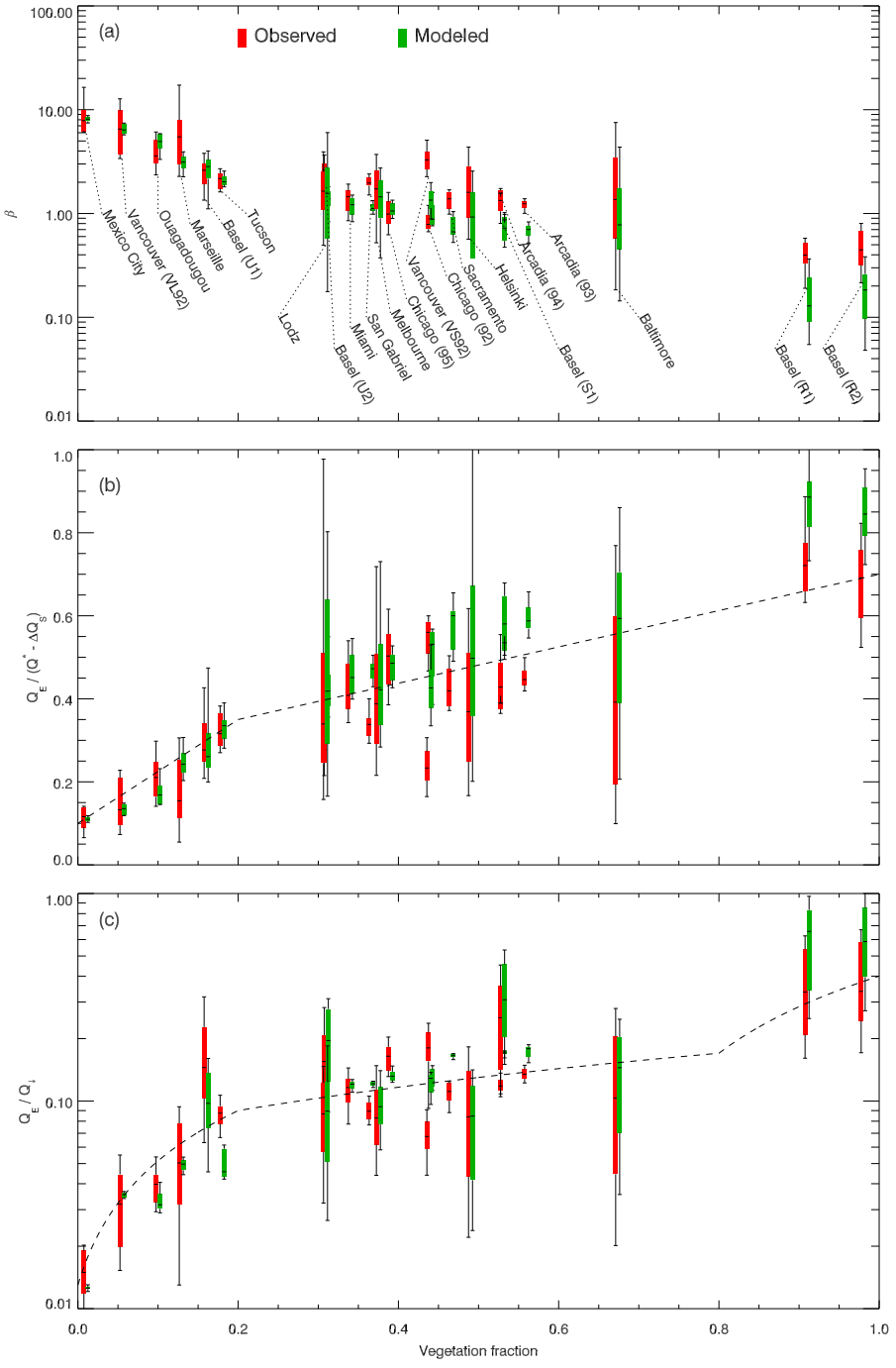

FIG. 8. Midday (1000–1400 LST) variability of observed and modeled (a) Bowen ratio, (b) latent heat scaled by available energy [Q^* minus the net storage heat flux ΔQ_s, ignoring the anthropogenic heat flux (i.e., Q_F)], and (c) latent heat flux scaled by incoming all-wave radiation $Q_\downarrow$, shown with the interquartile range (box), median (center lines), and 10th and 90th percentiles (whiskers). Linear dashed lines have no significance and are purely a visual guide.

there are future observational campaigns for such environments or if observational data are analyzed according to wind sectors that have differing plan area vegetation fractions. Future observational campaigns need to be long term in order to sample a range of synoptic and climatic extremes, so that the nature of the variability and sequencing can be evaluated for their impacts on the surface fluxes.

Acknowledgments. M.J. Best was supported by the Joint DECC/Defra Met Office Hadley Centre Climate Programme (CA01101). C.S.B. Grimmond was supported by the Met Office/Newton Fund Climate Science for Services Partnership: China. Funds to support PILPS-Urban were provided by the Met Office (P001550). We thank Leena Järvi for enabling us to use the Helsinki data and Andreas Christen and Andy Coutts for their helpful comments and enabling us to use the Basel and Melbourne data, respectively. We also thank all those who funded the observations and were involved in the collection and processing of the data.

REFERENCES

Best, M. J., 2005: Representing urban areas within operational numerical weather prediction models. *Bound.-Layer Meteor.*, **114**, 91–109, doi:10.1007/s10546-004-4834-5.

——, and C. S. B. Grimmond, 2013: Analysis of the seasonal cycle within the first international urban land surface model comparison. *Bound.-Layer Meteor.*, **146**, 421–446, doi:10.1007/s10546-012-9769-7.

——, and ——, 2014: Importance of initial state and atmospheric conditions for urban land surface models performance. *Urban Climate*, **10**, 387–406, doi:10.1016/j.uclim.2013.10.006.

——, and ——, 2015: Key conclusions of the first international urban land surface model comparison. *Bull. Amer. Meteor. Soc.*, **96**, 805–819, doi:10.1175/BAMS-D-14-00122.1.

——, and ——, 2016: Investigation of the impact of anthropogenic heat flux within an urban land surface model and PILPS-Urban. *Theor. Appl. Climatol.*, doi:10.1007/s00704-015-1554-3, in press.

——, ——, and M. G. Villani, 2006: Evaluation of the urban tile in MOSES using surface energy balance observations. *Bound.-Layer Meteor.*, **118**, 503–525, doi:10.1007/s10546-005-9025-5.

——, and Coauthors, 2011: The Joint UK Land Environment Simulator (JULES), model description—Part 1: Energy and water fluxes. *Geosci. Model Dev.*, **4**, 677–699, doi:10.5194/gmd-4-677-2011.

——, and Coauthors, 2015: The plumbing of land surface models: Benchmarking model performance. *J. Hydrometeor.*, **16**, 1425–1442, doi:10.1175/JHM-D-14-0158.1.

Christen, A., and R. Vogt, 2004: Energy and radiation balance of a central European city. *Int. J. Climatol.*, **24**, 1395–1421, doi:10.1002/joc.1074.

Collatz, G. J., J. T. Ball, C. Grivet, and J. A. Berry, 1991: Physical and environmental regulation of stomatal conductance, photosynthesis and transpiration: A model that includes a laminar boundary layer. *Agric. For. Meteor.*, **54**, 107–136, doi:10.1016/0168-1923(91)90002-8.

——, M. Ribas-Carbo, and J. A. Berry, 1992: Coupled phytosynthesis–stomatal conductance model for leaves of C_4 plants. *Aust. J. Plant Physiol.*, **19**, 519–538, doi:10.1071/PP9920519.

Coutts, A. M., J. Beringer, and N. J. Tapper, 2007a: Characteristics influencing the variability of urban CO_2 fluxes in Melbourne, Australia. *Atmos. Environ.*, **41**, 51–62, doi:10.1016/j.atmosenv.2006.08.030.

——, ——, and ——, 2007b: Impact of increasing urban density on local climate: Spatial and temporal variations in the surface energy balance in Melbourne, Australia. *J. Appl. Meteor.*, **46**, 477–493, doi:10.1175/JAM2462.1.

Crawford, B., C. S. B. Grimmond, and A. Christen, 2011: Five years of carbon dioxide fluxes measurements in a highly vegetated suburban area. *Atmos. Environ.*, **45**, 896–905, doi:10.1016/j.atmosenv.2010.11.017.

Dee, D. P., and Coauthors, 2011: The ERA-Interim reanalysis: Configuration and performance of the data assimilation system. *Quart. J. Roy. Meteor. Soc.*, **137**, 553–597, doi:10.1002/qj.828.

Dupont, S., and P. G. Mestayer, 2006: Parameterisation of the urban energy budget with the submesoscale soil model. *J. Appl. Meteor. Climatol.*, **45**, 1744–1765, doi:10.1175/JAM2417.1.

Fortuniak, K., 2003: A slab surface energy balance model (SUEB) and its application to the study on the role of roughness length in forming an urban heat island. *Acta Univ. Wratislav.*, **2542**, 368–377.

Grimmond, C. S. B., and T. R. Oke, 1986: Urban water balance. 2. Results from a suburb of Vancouver, British Columbia. *Water Resour. Res.*, **22**, 1404–1412, doi:10.1029/WR022i010p01404.

——, and ——, 1995: Comparison of heat fluxes from summertime observations in the suburbs of four North American cities. *J. Appl. Meteor.*, **34**, 873–889, doi:10.1175/1520-0450(1995)034<0873:COHFFS>2.0.CO;2.

——, and ——, 1999: Heat storage in urban areas: Local-scale observations and evaluation of a simple model. *J. Appl. Meteor.*, **38**, 922–940, doi:10.1175/1520-0450(1999)038<0922:HSIUAL>2.0.CO;2.

——, and ——, 2002: Turbulent heat fluxes in urban areas: Observations and Local-Scale Urban Meteorological Parameterization Scheme (LUMPS). *J. Appl. Meteor.*, **41**, 792–810, doi:10.1175/1520-0450(2002)041<0792:THFIUA>2.0.CO;2.

——, and A. Christen, 2012: Flux measurements in urban ecosystems. *FluxLetter: The Newsletter of Fluxnet*, Vol. 5, No. 1, University of California, Berkeley, Berkley, CA, 1–8.

——, T. R. Oke, and H. A. Cleugh, 1993: The role of 'rural' in comparisons of observed suburban–rural flux differences. *IAHS Publ.*, **212**, 165–174.

——, C. Souch, and M. D. Hubble, 1996: Influence of tree cover on summertime surface energy balance fluxes, San Gabriel Valley, Los Angeles. *Climate Res.*, **6**, 45–57, doi:10.3354/cr006045.

——, J. A. Salmond, T. R. Oke, B. Offerle, and A. Lemonsu, 2004: Flux and turbulence measurements at a densely built-up site in Marseille: Heat, mass (water and carbon dioxide), and momentum. *J. Geophys. Res.*, **109**, D24101, doi:10.1029/2004JD004936.

——, and Coauthors, 2010: The international urban energy balance models comparison project: First results from phase 1. *J. Appl. Meteor. Climatol.*, **49**, 1268–1292, doi:10.1175/2010jamc2354.1.

——, and Coauthors, 2011: Initial results from phase 2 of the international urban energy balance model comparison. *Int. J. Climatol.*, **31**, 244–272, doi:10.1002/joc.2227.

Harris, I., P. D. Jones, T. J. Osborn, and D. H. Lister, 2014: Updated high-resolution grids of monthly climatic observations—The CRU TS3.10 dataset. *Int. J. Climatol.*, **34**, 623–642, doi:10.1002/joc.3711.

Järvi, L., C. S. B. Grimmond, M. Taka, A. Nordbo, H. Setälä, and I. B. Strachan, 2014: Development of the surface urban energy and water balance scheme (SUEWS) for cold climate cities. *Geosci. Model Dev.*, **7**, 1691–1711, doi:10.5194/gmd-7-1691-2014.

Kawai, T., M. K. Ridwan, and M. Kanda, 2009: Evaluation of the simple urban energy balance model using 1-yr flux observations at two cities. *J. Appl. Meteor. Climatol.*, **48**, 693–715, doi:10.1175/2008JAMC1891.1.

King, T., and C. S. B. Grimmond, 1997: Transfer mechanisms over an urban surface for water vapor, sensible heat, and momentum.

Preprints, *12th Conf. on Boundary Layers and Turbulence*, Vancouver, BC, Canada, Amer. Meteor. Soc., 455–456.

Kondo, H., Y. Genchi, Y. Kikegawa, Y. Ohashi, H. Yoshikado, and H. Komiyama, 2005: Development of a multi-layer urban canopy model for the analysis of energy consumption in a big city: Structure of the urban canopy model and its basic performance. *Bound.-Layer Meteor.*, **116**, 395–421, doi:10.1007/s10546-005-0905-5.

Krayenhoff, E. S., and J. A. Voogt, 2007: A microscale three-dimensional urban energy balance model for studying surface temperatures. *Bound.-Layer Meteor.*, **123**, 433–461, doi:10.1007/s10546-006-9153-6.

Lee, S.-H., and S.-U. Park, 2008: A vegetated urban canopy model for meteorological and environmental modelling. *Bound.-Layer Meteor.*, **126**, 73–102, doi:10.1007/s10546-007-9221-6.

Leuning, R., E. van Gorsel, W. J. Massman, and P. R. Isacc, 2012: Reflections on the surface energy imbalance problem. *Agric. For. Meteor.*, **156**, 65–74, doi:10.1016/j.agrformet.2011.12.002.

Loridan, T., and C. S. B. Grimmond, 2012a: Characterization of energy flux partitioning in urban environments: Links with surface seasonal properties. *J. Appl. Meteor. Climatol.*, **51**, 219–241, doi:10.1175/JAMC-D-11-038.1.

——, and ——, 2012b: Multi-site evaluation of an urban land-surface model: Intra-urban heterogeneity, seasonality and parameter complexity requirements. *Quart. J. Roy. Meteor. Soc.*, **138**, 1094–1113, doi:10.1002/qj.963.

——, ——, B. D. Offerle, D. T. Young, T. E. L. Smith, L. Järvi, and F. Lindberg, 2011: Local-Scale Urban Meteorological Parameterization Scheme (LUMPS): Longwave radiation parameterization and seasonality-related developments. *J. Appl. Meteor. Climatol.*, **50**, 185–202, doi:10.1175/2010JAMC2474.1.

Martilli, A., A. Clappier, and M. W. Rotach, 2002: An urban surface exchange parameterisation for mesoscale models. *Bound.-Layer Meteor.*, **104**, 261–304, doi:10.1023/A:1016099921195.

Masson, V., 2000: A physically-based scheme for the urban energy budget in atmospheric models. *Bound.-Layer Meteor.*, **94**, 357–397, doi:10.1023/A:1002463829265.

Meier, F., and D. Scherer, 2012: Spatial and temporal variability of urban tree canopy temperature during summer 2010 in Berlin, Germany. *Theor. Appl. Climatol.*, **110**, 373–384, doi:10.1007/s00704-012-0631-0.

Monin, A. S., and A. M. Obukhov, 1954: Basic regularity in turbulent mixing in the surface layer of the atmosphere. *Tr. Geofiz. Inst., Akad. Nauk SSSR*, **24**, 163–187.

New, M., M. Hulme, and P. Jones, 1999: Representing twentieth-century space–time climate variability. Part I: Development of a 1961–90 mean monthly terrestrial climatology. *J. Climate*, **12**, 829–856, doi:10.1175/1520-0442(1999)012<0829:RTCSTC>2.0.CO;2.

——, ——, and ——, 2000: Representing twentieth-century space–time climate variability. Part II: Development of 1901–96 monthly grids of terrestrial surface climate. *J. Climate*, **13**, 2217–2238, doi:10.1175/1520-0442(2000)013<2217:RTCSTC>2.0.CO;2.

Newton, T., 1999: Energy balance fluxes in a subtropical city: Miami, FL. M.S. thesis, Dept. of Geography, University of British Columbia, 140 pp.

——, T. R. Oke, C. S. B. Grimmond, and M. Roth, 2007: The suburban energy balance in Miami, Florida. *Geogr. Ann.*, **89A**, 331–347, doi:10.1111/j.1468-0459.2007.00329.x.

Offerle, B., C. S. B. Grimmond, and K. Fortuniak, 2005a: Heat storage and anthropogenic heat flux in relation to the energy balance of a central European city centre. *Int. J. Climatol.*, **25**, 1405–1491, doi:10.1002/joc.1198.

——, P. Jonsson, I. Eliasson, and C. S. B. Grimmond, 2005b: Urban modification of the surface energy balance in the West African Sahel: Ouagadougou, Burkina Faso. *J. Climate*, **18**, 3983–3995, doi:10.1175/JCLI3520.1.

——, C. S. B. Grimmond, K. Fortuniak, K. Kłysik, and T. R. Oke, 2006a: Temporal variations in heat fluxes over a central European city centre. *Theor. Appl. Climatol.*, **84**, 103–115, doi:10.1007/s00704-005-0148-x.

——, ——, ——, and W. Pawlak, 2006b: Intraurban differences of surface energy fluxes in a central European city. *J. Appl. Meteor. Climatol.*, **45**, 125–136, doi:10.1175/JAM2319.1.

Oke, T. R., and J. E. Hay, 1998: *The Climate of Vancouver.* 2nd ed. BC Geographical Series, No. 50, University of British Columbia Press, 84 pp.

——, A. Spronken-Smith, E. Jauregui, and C. S. B. Grimmond, 1999: The energy balance of central Mexico City during the dry season. *Atmos. Environ.*, **33**, 3919–3930, doi:10.1016/S1352-2310(99)00134-X.

Oleson, K. W., G. B. Bonan, J. Feddema, M. Vertenstein, and C. S. B. Grimmond, 2008: An urban parameterization for a global climate model: 1. Formulation and evaluation for two cities. *J. Appl. Meteor. Climatol.*, **47**, 1038–1060, doi:10.1175/2007JAMC1597.1.

Pawlak, W., K. Fortuniak, and M. Siedlecki, 2011: Carbon dioxide flux in the centre of Łódź, Poland—Analysis of a 2-year eddy covariance measurement data set. *Int. J. Climatol.*, **31**, 232–243, doi:10.1002/joc.2247.

Porson, A., P. A. Clark, I. N. Harman, M. J. Best, and S. E. Belcher, 2010: Implementation of a new urban scheme in the MetUM. Part I: Description and idealized simulations. *Quart. J. Roy. Meteor. Soc.*, **136**, 1514–1529, doi:10.1002/qj.668.

Ryu, Y.-H., J.-J. Baik, and S.-H. Lee, 2011: A new single layer urban canopy model for use in mesoscale atmospheric models. *J. Appl. Meteor. Climatol.*, **50**, 1773–1794, doi:10.1175/2011JAMC2665.1.

Schneider, U., A. Becker, P. Finger, A. Meyer-Christoffer, M. Ziese, and B. Rudolf, 2014: GPCC's new land surface precipitation climatology based on quality-controlled in situ data and its role in quantifying the global water cycle. *Theor. Appl. Climatol.*, **115**, 15–40, doi:10.1007/s00704-013-0860-x.

Sheng, J., and F. Zwiers, 1998: An improved scheme for time-dependent boundary conditions in atmospheric general circulation models. *Climate Dyn.*, **14**, 609–613, doi:10.1007/s003820050244.

Stewart, I. D., and T. R. Oke, 2012: Local climate zones for urban temperature studies. *Bull. Amer. Meteor. Soc.*, **93**, 1879–1900, doi:10.1175/BAMS-D-11-00019.1.

Vesala, T., and Coauthors, 2008: Surface–atmosphere interactions over complex urban terrain in Helsinki, Finland. *Tellus*, **60B**, 188–199, doi:10.1111/j.1600-0889.2007.00312.x.

Weedon, G. P., and Coauthors, 2011: Creation of the WATCH Forcing Data and its use to assess global and regional reference crop evaporation over land during the twentieth century. *J. Hydrometeor.*, **12**, 823–848, doi:10.1175/2011JHM1369.1.

——, G. Balsamo, N. Bellouin, S. Gomes, M. J. Best, and P. Viterbo, 2014: The WFDEI meteorological forcing data set: WATCH Forcing Data methodology applied to ERA-Interim reanalysis data. *Water Resour. Res.*, **50**, 7505–7514, doi:10.1002/2014WR015638.